Atmospheric Research 302 (2024) 107303

Contents lists available at ScienceDirect

Atmospheric Research

journal homepage: www.elsevier.com/locate/atmosres

Quantitative analysis of sulfate formation from crop burning in Northeast China: Unveiling the primary processes and transboundary transport to South Korea

Dongjin Kim [a,b], Yunsoo Choi [c], Wonbae Jeon [b,d,*], Jeonghyeok Mun [a], Jaehyeong Park [a], Cheol-Hee Kim [b,d,e], Jung-Woo Yoo [e]

[a] Division of Earth Environmental System, Pusan National University, Busan 46241, Republic of Korea
[b] BK21 School of Earth and Environmental Systems, Pusan National University, Busan 46241, Republic of Korea
[c] Department of Earth and Atmospheric Sciences, University of Houston, Houston, TX 77204, USA
[d] Department of Atmospheric Sciences, Pusan National University, Busan 46241, Republic of Korea
[e] Institute of Environmental Studies, Pusan National University, Busan 46241, Republic of Korea

ARTICLE INFO

Keywords:
Crop burning
FINN
CMAQ
Sulfate
Transboundary transport

ABSTRACT

The substantial amount of pollutants produced by crop burning leads to particulate matter ($PM_{2.5}$) formation through chemical reactions in the atmosphere. In this study, we quantitatively examined the characteristics of $PM_{2.5}$ component concentration changes and the production mechanism of sulfate (SO_4^{2-}) due to crop burning in China, during a period of high $PM_{2.5}$ concentrations in South Korea. Crop burning emissions were obtained from the Fire INventory from NCAR (FINN), and simulations were conducted using the Community Multi-scale Air Quality (CMAQ) model. The concentrations of $PM_{2.5}$, nitrate, ammonium, organic carbon, and elemental carbon caused by crop burning were the highest in Northeast China, while the SO_4^{2-} concentration was higher in the Shandong Peninsula and the Yellow Sea. SO_4^{2-} was mainly produced through the oxidation reaction by hydrogen peroxide (H_2O_2) ($H_2O_2 + S(IV) = S(VI) + H_2O$) (1.44 μg/m^3, 80.49%). H_2O_2 that contributed to SO_4^{2-} production was primarily produced through the self-reaction of hydroperoxy radical (HO_2). Moreover, HO_2, which contributed to the production of H_2O_2, was mainly formed through the decomposition of peroxynitric acid (PNA), which is produced by nitric oxide (NO_x) emissions from crop burning. SO_4^{2-} in the Yellow Sea was reported to be predominantly produced by the oxidation of sulfur dioxide (SO_2) by hydroxyl radical (OH) ($OH + SO_2 = SULF + HO_2$); however, our study suggests that the PNA formed by NO_x emissions from crop burning could contribute to an increase in H_2O_2, which subsequently promotes SO_4^{2-} production. The produced SO_4^{2-} was then transported across the Yellow Sea, impacting the elevated $PM_{2.5}$ concentrations in Jeju Island, a suburban area of South Korea. These findings demonstrate that the mechanisms of SO_4^{2-} production by crop burning emissions differ from those of anthropogenic emissions.

1. Introduction

Biomass burning occurs in various forms, including wildfire, crop burning, and waste burning (Akagi et al., 2011), and it emits many pollutants. These include fine particulate matter ($PM_{2.5}$), nitrogen oxides (NO_x), sulfur oxides (SO_x), ammonia (NH_3), and volatile organic compounds (VOCs) (Zhou et al., 2017). Pollutants emitted by biomass burning can alter the chemical properties of the surrounding atmosphere (Yin et al., 2019a), and can affect air quality in distant regions through long-range transport if they remain in the atmosphere for prolonged periods (Val Martin et al., 2006; Akagi et al., 2012). Lin et al. (2014) reported that biomass burning in the Indochinese Peninsula of Southeast Asia during the spring seasons of 2006 and 2009 resulted in elevated concentrations of carbon monoxide (CO), ozone (O_3), and PM_{10} in central Taiwan. Similarly, Johnson et al. (2021) reported that Siberian biomass burning that occurred during the summer of 2019 increased CO and $PM_{2.5}$ concentrations in western Canada.

Approximately 23% of global biomass burning emissions are

* Corresponding authors at: Department of Atmospheric Sciences, Pusan National University, Busandaehak-ro 63beon-gil, Geumjeong-gu, Busan 46241, Republic of Korea.
E-mail address: wbjeon@pusan.ac.kr (W. Jeon).

https://doi.org/10.1016/j.atmosres.2024.107303
Received 12 October 2023; Received in revised form 30 December 2023; Accepted 19 February 2024
Available online 21 February 2024

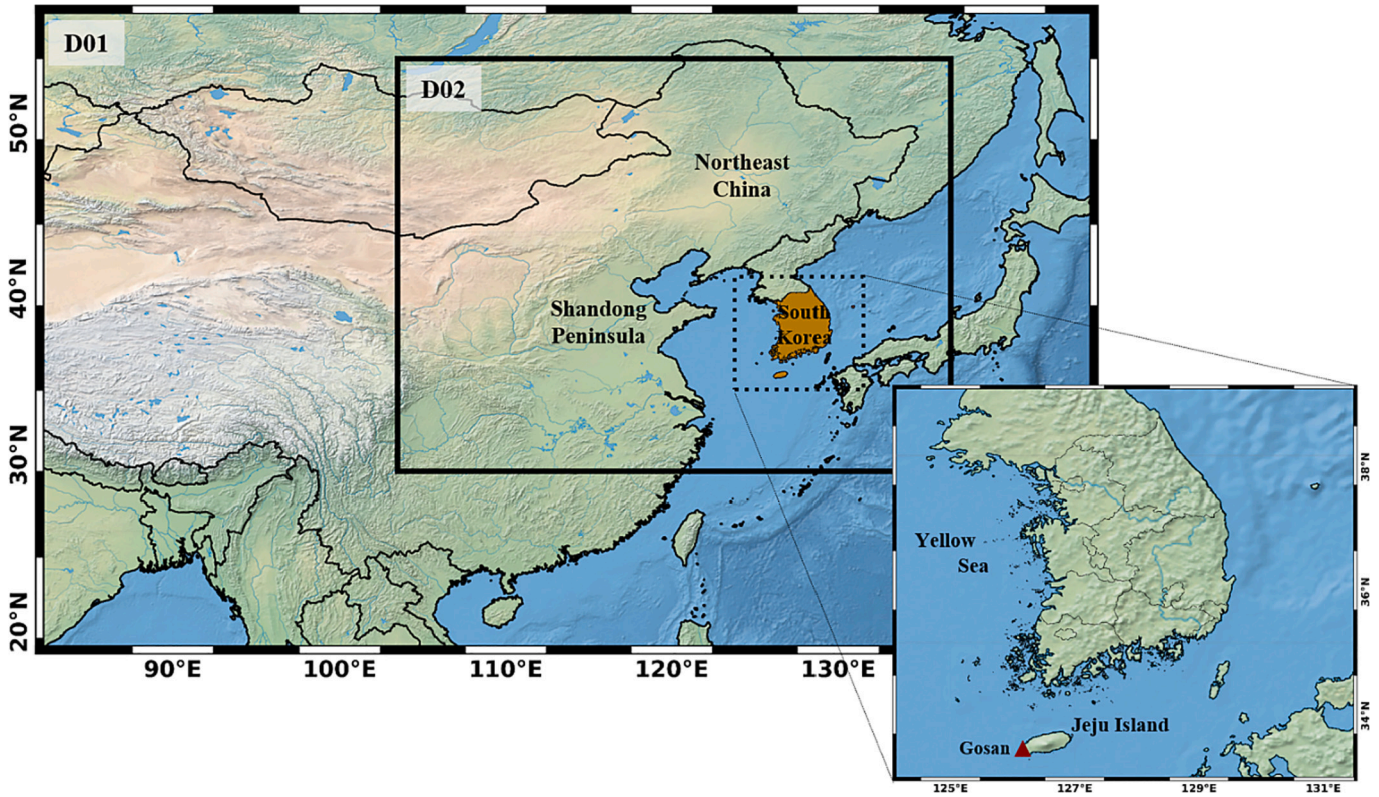

Fig. 1. Domains of numerical simulations for Weather Research and Forecasting (WRF) and Community Multi-scale Air Quality (CMAQ). The triangle in the right panel indicates the Gosan observation site in South Korea.

attributed to crop burning (Yadav and Devi, 2019), which is a major source of pollutants such as particulate matter, greenhouse gases, and trace gases (Zhou et al., 2018a; Hong et al., 2023). Therefore, numerous studies have analyzed the impact of pollutants released into the atmosphere through crop burning on air quality. Yamaji et al. (2010) found that crop burning in Central Eastern China in June 2006 significantly impacted pollutant concentrations in the region. In this case, the concentrations of O_3, organic carbon (OC), CO, and black carbon at the summit of Mount Tai in China increased by 26%, 80%, 62%, and 79% compared to normal levels, respectively. Zhou et al. (2018b) reported that crop burning in October 2014 contributed approximately 19% to surface $PM_{2.5}$ concentrations in Beijing, China, and 40% and 29% to major $PM_{2.5}$ and OC concentrations, respectively.

Despite many studies quantitatively analyzing changes in the concentrations of $PM_{2.5}$, OC, and O_3 due to crop burning emissions, there is a relative lack of detailed research focusing on the production mechanisms of inorganic species like nitrate (NO_3^-), sulfate (SO_4^{2-}), and ammonium (NH_4^+). These species constitute a significant portion of $PM_{2.5}$. In particular, NO_x, SO_2, and NH_3 emitted from pollution sources are major precursors of NO_3^-, SO_4^{2-}, and NH_4^+, which can contribute to $PM_{2.5}$ concentrations by producing NO_3^-, SO_4^{2-}, and NH_4^+ through chemical reactions during pollutant transport (Kai et al., 2007; Cao et al., 2017).

Thus, understanding the changes in $PM_{2.5}$ concentrations due to crop burning emissions necessitates a detailed investigation of the production mechanisms for each $PM_{2.5}$ constituent. In this study, we conducted a quantitative analysis to assess the impact of crop burning on the elevated concentrations of $PM_{2.5}$ observed in South Korea in November 2015. We used the Fire INventory from NCAR (FINN) —a high-resolution biomass burning emissions inventory provided by the National Center for Atmospheric Research (NCAR)— to extract crop burning emission data. Subsequently, we conducted numerical simulation experiments with and without crop burning emissions using the Community Multi-scale Air Quality (CMAQ), a three-dimensional photochemical transport model. To investigate thoroughly the mechanisms involved in the production of $PM_{2.5}$ components, we utilized the sulfur tracking model (STM) and integrated reaction rate (IRR) provided by CMAQ.

2. Material and methods

2.1. Study region

Northeast Asia, including South Korea, is a region frequently experiencing high concentrations of air pollutants due to the prevalent transboundary transport of pollutants (e.g., Kim et al., 2017; Lee et al., 2022). The transboundary transport of pollutants to South Korea often occurs in conjunction with favorable meteorological conditions, a phenomenon explored in previous studies (Lee et al., 2015a; Jeon et al., 2018a; Bae et al., 2020; Jeon et al., 2021). The Gosan site, located on Jeju Island, South Korea, serves as a national background monitoring location for studying the long-range transport of pollutants from Northeast Asia, as it is less impacted by anthropogenic emissions (Moon et al., 2008; Kim et al., 2012; Lee et al., 2015b). However, at 05 UTC on November 9, 2015, the Gosan site recorded a PM_{10} concentration of 147 $\mu g/m^3$, surpassing the threshold for issuing a particulate matter advisory in South Korea (no observational data for $PM_{2.5}$ concentrations were available during this period). Prolonged exposure to such high PM concentrations can lead to serious illnesses, including respiratory diseases (Xu et al., 2016; Yeo and Kim, 2019; Kyung and Jeong, 2020). During this period of high PM_{10} concentrations in South Korea, significant crop burning was observed in Northeast China with 2291, 1050, and 1109 spots identified from November 4 to 6, 2015 (Yin et al., 2019b; Lee et al., 2021). Additionally, Zhang et al. (2017) reported extraordinary $PM_{2.5}$ concentrations of 1326 $\mu g/m^3$ in Shenyang on November 8, 2015, during the agricultural off-season in Northeast China. Pollutants emitted by these crop burnings could have contributed to the elevated

PM_{10} concentrations at the Gosan site through transboundary transport. Therefore, we analyzed the impact of crop burning in Northeast China on the high PM_{10} concentrations at the Gosan site.

2.2. Model configuration

2.2.1. Meteorological and photochemical transport model

We utilized the CMAQ (v5.3.2, Byun and Schere, 2006; Appel et al., 2021), a three-dimensional photochemical transport model developed by the U.S. Environmental Protection Agency, to conduct air quality numerical simulations studying the impacts of crop burning emissions. The simulation domain, D01, encompassed a broad region of East Asia at a 45 km resolution (128 × 98 grids) to generate initial and boundary conditions. D02 was simulated at a 15 km resolution (179 × 182 grids), covering Northeast China, where crop burning occurred, and South Korea, where the Gosan site is located (Fig. 1). Anthropogenic and biogenic emissions were generated using the Emissions Database for Global Atmospheric Research (v6.1, Crippa et al., 2022) and the Model of Emissions of Gases and Aerosols from Nature (v2.1, Guenther et al., 2012), respectively. For crop burning emissions, we used FINN (v1.5, Wiedinmyer et al., 2011), which provides high-resolution (1 km) daily estimates of biomass burning emissions and is widely used as emission input data for chemical transport models (Jeon et al., 2018b; Xu et al., 2018; Kim et al., 2022). Since the emissions in FINN were classified into seven vegetation types burned at each pixel (Table S1) (Friedl et al., 2010), we specifically selected emissions categorized as croplands (GENVEG = 9). In this study, we conducted an experiment that included all crop burning emissions in China (CROP) and compared it with an experiment that excluded crop burning emissions (BASE). However, crop burning was observed at 4450 spots in Northeast China from November 4 to 6, 2015 (as mentioned in Section 2.1), which is approximately 3.9 times higher than the number of crop burning spots (1150) in the FINN data. As a result, we conducted an additional simulation (rCROP) by scaling the crop burning emissions in the FINN data by the difference from the observed data. In addition, an extra sensitivity simulation was designed to assess the impact of NO_x emitted from crop burning on the SO_4^{2-} production mechanism. We reduced the NO_x emissions from crop burning used in the rCROP experiment by 50% (rCROP_NO_x) and analyzed the concentration changes of substances contributing to SO_4^{2-} production. For the CMAQ simulations, we applied the CB6r3 and AERO7 for the gas and aerosol phase chemical mechanisms, respectively.

The meteorological input data of the CMAQ were generated using the Weather Research and Forecasting (WRF; v4.1.1, Skamarock et al., 2019) model in conjunction with the Meteorology-Chemistry Interface Processor (v5.1, Otte and Pleim, 2010). The initial and boundary conditions of the WRF model were sourced from the European Centre for Medium-range Weather Forecasts ERA5 reanalysis data with a horizontal resolution of 0.25° × 0.25° at 6-h intervals. Additionally, we applied grid and observational nudging to enhance the accuracy of meteorological simulations (Stauffer and Seaman, 1990; Liu et al., 2008; Jeon et al., 2015). The simulation spanned from 00 UTC on October 25, 2015, to 00 UTC on November 18, 2015, considering the initial and boundary conditions and including the period of high PM_{10} concentration at the Gosan site. The detailed options employed for the WRF and CMAQ simulations are presented in Tables S2 and S3, respectively.

To quantitatively analyze the processes of the $PM_{2.5}$ production mechanism, we employed the STM and IRR, which are provided by the CMAQ model (Gipson, 1999; Liu et al., 2010; Itahashi et al., 2018; Jeon et al., 2021). The STM was used to estimate the contributions of chemical reactions, emissions, initial/boundary conditions, and other factors to the overall SO_4^{2-} concentration, while the IRR was used to conduct a detailed analysis of the contributions of all chemical reactions involved in the formation of the gaseous species.

2.2.2. Atmospheric trajectory model

The HYbrid Single-Particle Lagrangian Integrated Trajectory (HYSPLIT; v4, Draxler, 1999; Stein et al., 2015) model from the National Oceanic and Atmospheric Administration was used to identify the trajectories of pollutants reaching the Gosan site in South Korea. The HYSPLIT model is a comprehensive tool for computing complex transport, dispersion, chemical transformation, deposition, as well as simple air parcel trajectories, making it one of the most widely used atmospheric transport and dispersion models. Meteorological input data for HYSPLIT were generated using the WRF simulation results. Backward trajectory analysis was conducted at altitudes of 10, 100, and 1000 m over a 48-h period, starting at 05 UTC on November 9, 2015, when the peak PM_{10} concentrations ware observed at the Gosan site.

2.3. Observational data

Data from ground-based meteorological observation stations (39 in South Korea, 43 in China) and air quality monitoring stations (316 in South Korea, 1163 in China) located in the D02 domain were used to evaluate the accuracy of the WRF and CMAQ models. The validation process included comparisons of temperature and wind speed for the WRF model, and of PM_{10} and $PM_{2.5}$ for the CMAQ (BASE experiment). The statistical parameters used for verification included the root mean squared error (RMSE) and mean bias error (MBE), both of which assess the discrepancy between observations and the model. The index of agreement (IOA) and the correlation coefficient (R) were used to evaluate the model's accuracy to the observations' temporal variability. Detailed formulas for each parameter are provided in the Supplementary Materials.

Additionally, to investigate the dispersion of pollutants induced by crop burning, we utilized land aerosol optical depth (AOD) data from the Moderate Resolution Imaging Spectroradiometer (MODIS) sensor onboard the Terra and Aqua satellites of the National Aeronautics and Space Administration (Levy et al., 2017). AOD, which measures the extinction coefficient of light attenuation by atmospheric particles (Chen et al., 2022; Feng et al., 2023), serves as an indicator of atmospheric pollution and has been widely used to assess air pollution levels (Chu et al., 2003; Xie and Sun, 2021). In this study, we used daily level 2 AOD data with a spatial resolution of 1 km. The data were re-gridded to match the resolution of the D02 (15 km) in the CMAQ for analysis.

3. Results and Discussion

3.1. Evaluation of WRF and CMAQ model performance

Scatter plots and statistics comparing the WRF simulation with the observations are presented in Fig. S1. The results showed that the RMSEs for temperature and wind speed were 2.02 °C and 1.99 ms^{-1}, respectively, and MBEs were −0.58 °C and 1.19 ms^{-1}, respectively. This indicates a slight underestimation of the simulated temperature and a slight overestimation of the wind speed compared with observations. However, the IOAs for temperature and wind speed were 0.95 and 0.73, respectively, and the R values were 0.92 and 0.64, respectively. The verification results for the BASE experiment of the CMAQ are shown in Fig. S2. The RMSEs for PM_{10} and $PM_{2.5}$ were 21.86 μg/m^3 and 12.65 μg/m^3, respectively, and the MBEs were −19.45 μg/m^3 and − 7.25 μg/m^3, respectively. Although the CMAQ model underestimated the observations, the IOA values of 0.74 and 0.76, along with the R values of 0.87 and 0.75, indicated that the model effectively captured temporal variability. The verification results suggested that the WRF and CMAQ simulations successfully captured temporal variability of the observations, thus demonstrating their suitability for conducting experiments involving crop burning emissions.

In addition, we evaluated the experiments that included crop burning emissions (CROP and rCROP) discussed in Section 2.3 to assess whether the CMAQ model accurately simulated the influence of these

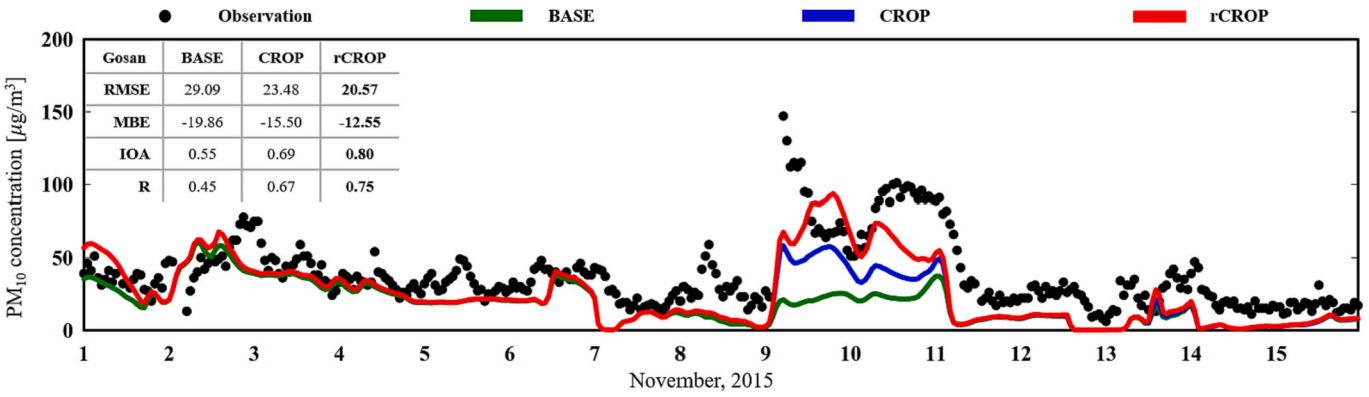

Fig. 2. Comparison of PM_{10} concentrations at the Gosan site in South Korea from the Community Multi-scale Air Quality (CMAQ) numerical simulations (BASE, CROP, rCROP) during the simulation period.

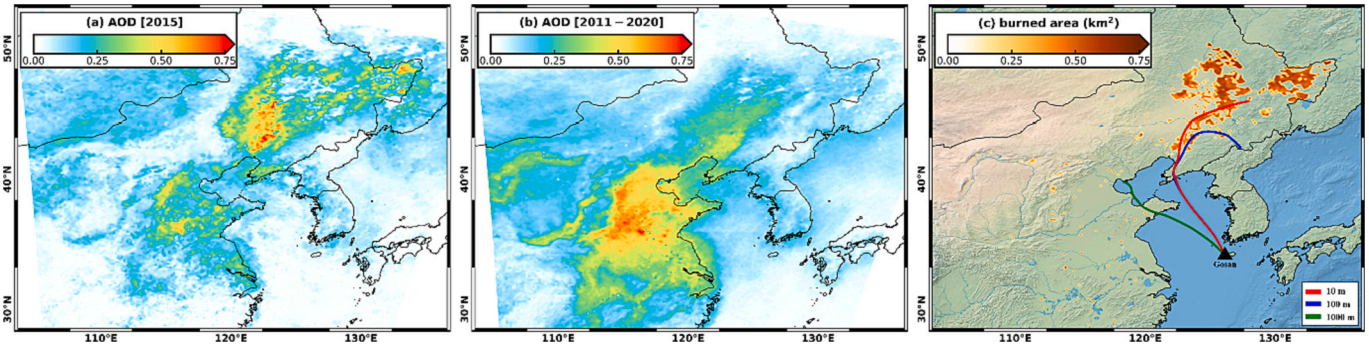

Fig. 3. (a) The 550-nm aerosol optical depth (AOD) observed by the Moderate Resolution Imaging Spectroradiometer (MODIS) from November 1 to 15, 2015, and (b) from 2011 to 2020. (c) Backward trajectory results at the Gosan site in South Korea and the area burned by crop burning according to the Fire INventory from NCAR (FINN) data (unit: km^2).

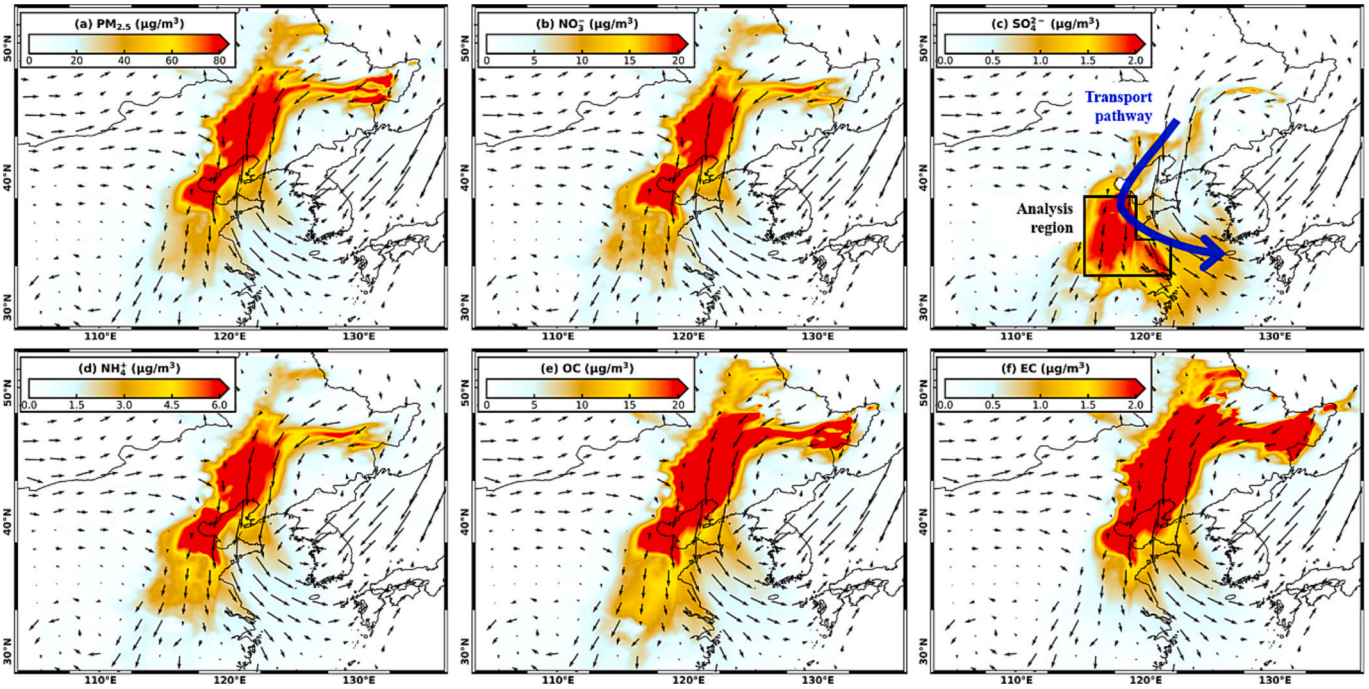

Fig. 4. Horizontal distribution of concentration levels for each pollutant induced by crop burning emissions. The values are averaged from the surface to the top of the plume during the analysis period.

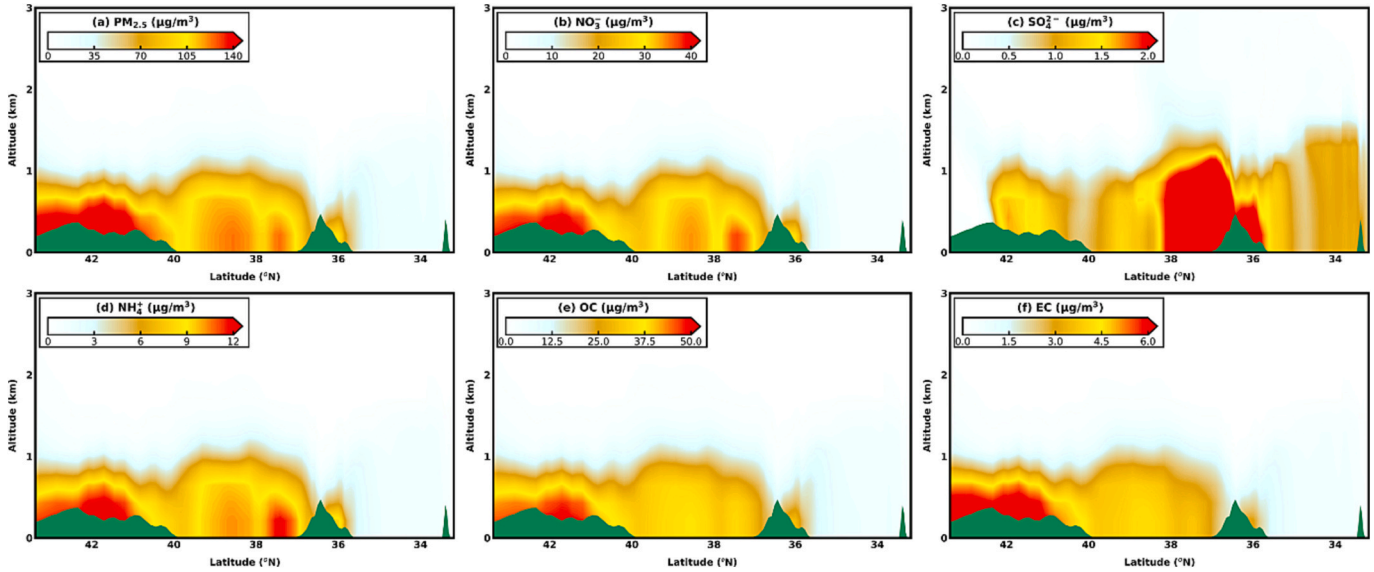

Fig. 5. Vertical distribution of concentrations for each pollutant influenced by crop burning emissions. The values are averaged along the transport pathway (Fig. 4 (c)) during the analysis period.

emissions. The validation was conducted at the Gosan site, and the observed PM_{10} concentrations were compared with those from the BASE, CROP, and rCROP experiments (Fig. 2). In the BASE and CROP experiments, the IOAs at the Gosan site were 0.55 and 0.69, respectively, and the R values were 0.45 and 0.67, respectively. In contrast, the IOA and R of PM_{10} concentrations in the rCROP experiment were 0.80 and 0.75, showing significant improvements in both RMSE and MBE. This indicates that the rCROP experiment achieved the most statistically significant results and effectively captured the temporal variations in PM_{10} concentrations. However, the maximum PM_{10} concentrations at the Gosan site were not simulated perfectly in the rCROP experiment. This could be attributed to the underestimation of crop burning emissions in Northeast China within the FINN data (Uranishi et al., 2019; Cheng et al., 2021). Therefore, in this study, we designated rCROP as the experiment that included crop burning emissions and compared it with the BASE experiment.

3.2. Analysis of backward trajectory and satellite data

The 550-nm AOD obtained from MODIS for the period from November 1 to 15, 2015, is shown in Fig. 3(a). Higher AOD values were observed in Northeast China and the Shandong Peninsula. The AOD in the Shandong Peninsula was primarily due to local emission sources (Li et al., 2017; Si et al., 2019), as indicated by the distribution of AOD within the domain from 2011 to 2020 (Fig. 3(b)). In contrast, the AOD in Northeast China displayed notably higher values during the simulation period, largely owing to significant emissions from crop burning. Fig. 3 (c) presents the results of the backward trajectory analysis at the Gosan site, conducted using the HYSPLIT model, alongside the burned area data from all crop burning in the FINN database. The trajectories suggested that pollutants reaching the Gosan site at heights of 10 and 100 m were transported from Northeast China, where numerous crop burning events were recorded. These results suggest that significant pollutants emitted from crop burning in Northeast China have affected air quality at the Gosan site and the surrounding areas.

3.3. Concentration changes in $PM_{2.5}$ and $PM_{2.5}$ components induced by crop burning emissions

To comprehensively analyze the changes in $PM_{2.5}$ concentrations and its major components (NO_3^-, SO_4^{2-}, NH_4^+, OC, and EC) caused by crop burning emissions, we calculated the difference between the rCROP and BASE experiments (i.e., rCROP minus BASE) and presented the horizontal distribution of each pollutant in Fig. 4. The analysis period, from 00 UTC on November 7, 2015, to 23 UTC on November 9, 2015, was chosen based on the transport period of pollutants emitted from crop burning and the time of high PM_{10} concentrations period at the Gosan site. Concentrations of each substance were averaged from the surface to the top of the plume during the analysis period.

The concentrations of $PM_{2.5}$, NO_3^-, NH_4^+, OC, and EC were the highest in Northeast China, where a substantial amount of crop burning occurred. However, the distribution of SO_4^{2-} concentration exhibited a different pattern compared to other substances. The high concentration of SO_4^{2-} was centered on the Shandong Peninsula, and it can be seen that the high concentration of SO_4^{2-} in that area was transported by northwesterly winds across the Yellow Sea to Jeju Island in South Korea. To more specifically identify the difference between SO_4^{2-} and other substances, the vertical distributions are displayed in Fig. 5. The concentrations of each pollutant were computed by averaging them along the pollutant transport pathway from Northeast China to Jeju Island depicted in Fig. 4(c) over the analysis period. The concentrations of $PM_{2.5}$, NO_3^-, NH_4^+, OC, and EC were high in Northeast China, where crop burning was concentrated. However, the SO_4^{2-} concentration was higher near the Shandong Peninsula, Yellow Sea, and Jeju Island, and this distribution of SO_4^{2-} might have influenced the high concentrations

Table 1
Contribution of each chemical reaction to the SO_4^{2-} concentration within the analysis region (Fig. 4(c)); the values are averaged from the surface to the top of the plume during the analysis period. The unit is μg/m^3, and values in parentheses indicate percentage (%) of the total.

BASE	
$H_2O_2 + S(IV) = S(VI) + H_2O$	0.45 (12.86)
$OH + SO_2 = SULF + HO_2$	1.52 (43.77)
rCROP	
$H_2O_2 + S(IV) = S(VI) + H_2O$	1.89 (35.85)
$OH + SO_2 = SULF + HO_2$	1.65 (31.34)
rCROP-BASE	
$H_2O_2 + S(IV) = S(VI) + H_2O$	1.44 (80.49)
$OH + SO_2 = SULF + HO_2$	0.13 (7.20)

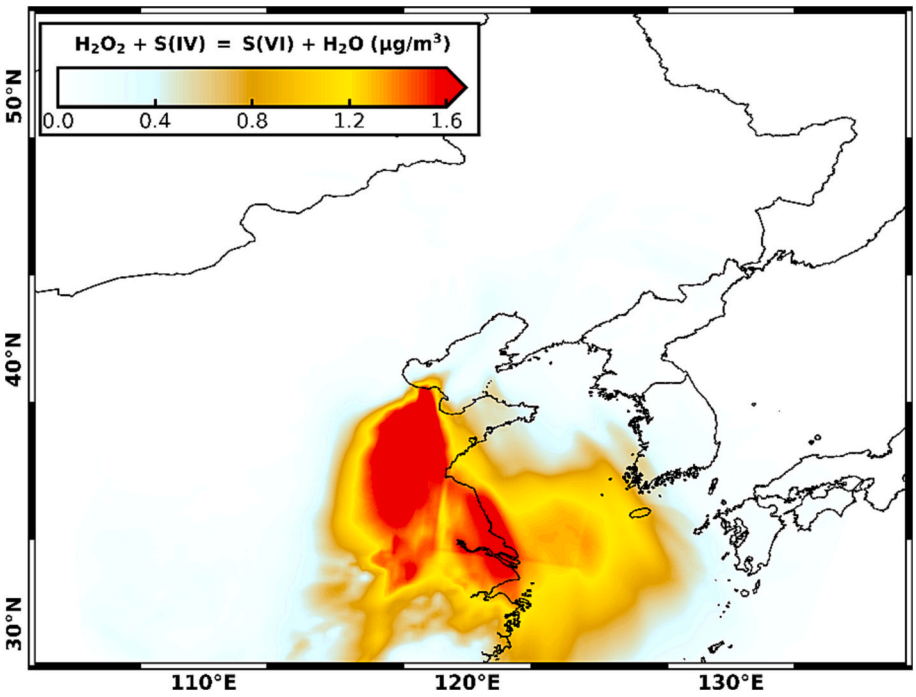

Fig. 6. Horizontal distribution of the $H_2O_2 + S(IV) = S(VI) + H_2O$ reaction, which contributed to the SO_4^{2-} production. The values were averaged from the surface to the top of the plume during the analysis period.

observed at the Gosan site. This suggests that, unlike other pollutants directly affected by crop burning emissions, the high concentration of SO_4^{2-} was produced through chemical processes under favorable conditions for SO_4^{2-} production near the Shandong Peninsula and the Yellow Sea. Therefore, a detailed analysis of the SO_4^{2-} production process in the area is necessary.

3.4. Analysis of the mechanism of sulfate production from crop burning emissions

3.4.1. Analysis of sulfate production reactions using STM

We utilized the STM of the CMAQ model to quantitatively analyze the SO_4^{2-} production process within the analysis region depicted in Fig. 4 (c). The primary chemical reactions contributing to SO_4^{2-} production in the BASE and rCROP experiments are presented in Table 1. In the BASE experiment, which did not include crop burning emissions, the dominant chemical reaction for SO_4^{2-} production was the reaction $OH + SO_2 = SULF + HO_2$ (Friedman et al., 2016), in which SO_2 is oxidized by hydroxyl (OH) radicals to form sulfate (1.52 μg/m^3,43.77%). This result is consistent with previous studies (Jeon et al., 2018b, 2021), which reported that SO_4^{2-} production during the transboundary transport of particulate matter from China to South Korea was dominated by the oxidation of SO_2 by OH. However, interestingly, in the rCROP experiment, which included crop burning emissions, the highest contribution was observed from the reaction $H_2O_2 + S(IV) = S(VI) + H_2O$ (Sarwar et al., 2013), in which hydrogen peroxide (H_2O_2) in the aqueous phase oxidizes S(IV) to produce accumulation-mode sulfate (1.89 μg/m^3, 35.85%). This suggests that H_2O_2, produced through atmospheric reactions during the transport of pollutants emitted from crop burning, contributed to the SO_4^{2-} concentration. To specifically assess the influence of crop burning emissions on SO_4^{2-} production, the differences between the two experiments (rCROP-BASE) were calculated and analyzed for each reaction. The primary chemical mechanism for SO_4^{2-} production due to crop burning emissions was found to be the $H_2O_2 + S(IV) = S(VI) + H_2O$ reaction (1.44 μg/m^3, 80.49%). The horizontal distribution of this reaction was high in East China and the Yellow Sea, aligning with the distribution of SO_4^{2-} concentration (Fig. 6). These findings imply that the mechanism of high concentration of SO_4^{2-} induced by crop burning emissions differs from that induced by anthropogenic emissions. It should be noted, however, that H_2O_2 is not a pollutant directly emitted by crop burning and is not included in the FINN data. Therefore, further investigation into the production of H_2O_2 is necessary to fully understand the mechanism of sulfate production by crop burning emissions.

Table 2
Contribution of each chemical reaction to the concentration of H_2O_2 and HO_2 within the analysis region (Fig. 4(c)). The values are averaged from the surface to the top of the plume during the analysis period.

[H_2O_2 production]	
$HO_2 + HO_2 = H_2O_2$	53.32%
$HO_2 + HO_2 + H_2O = H_2O_2$	42.07%
$OLE + O_3 = H_2O_2$	2.89%
$IOLE + O_3 = H_2O_2$	0.72%
[HO_2 production]	
$PNA = HO_2 + NO_2$	52.63%
$VOCs + M = HO_2$	30.04%
$CO + OH = HO_2$	7.84%
$HCO_3 = FORM + HO_2$	5.43%

3.4.2. Analysis of sulfate precursor production reactions using IRR

We used the IRR of the CMAQ model to identify the chemical production mechanisms of H_2O_2 as precursors of SO_4^{2-} (Table 2). H_2O_2 was mainly produced by the self-reaction of the hydroperoxyl (HO_2) radical ($HO_2 + HO_2 = H_2O_2$ and $HO_2 + HO_2 + H_2O = H_2O_2$), an important source of gas-phase H_2O_2 in the atmosphere (Stockwell, 1995) (54.32% and 42.07%, respectively). Additionally, terminal olefins (OLE) and internal olefins (IOLE), which are VOCs emitted from crop burning, contributed to the production of H_2O_2 through chemical reactions (2.89% and 0.72%, respectively). These results indicate that the production of H_2O_2 within the analysis region was primarily determined by HO_2 concentration. However, HO_2, which primarily contributes to the production of H_2O_2, is also not directly emitted from crop burning.

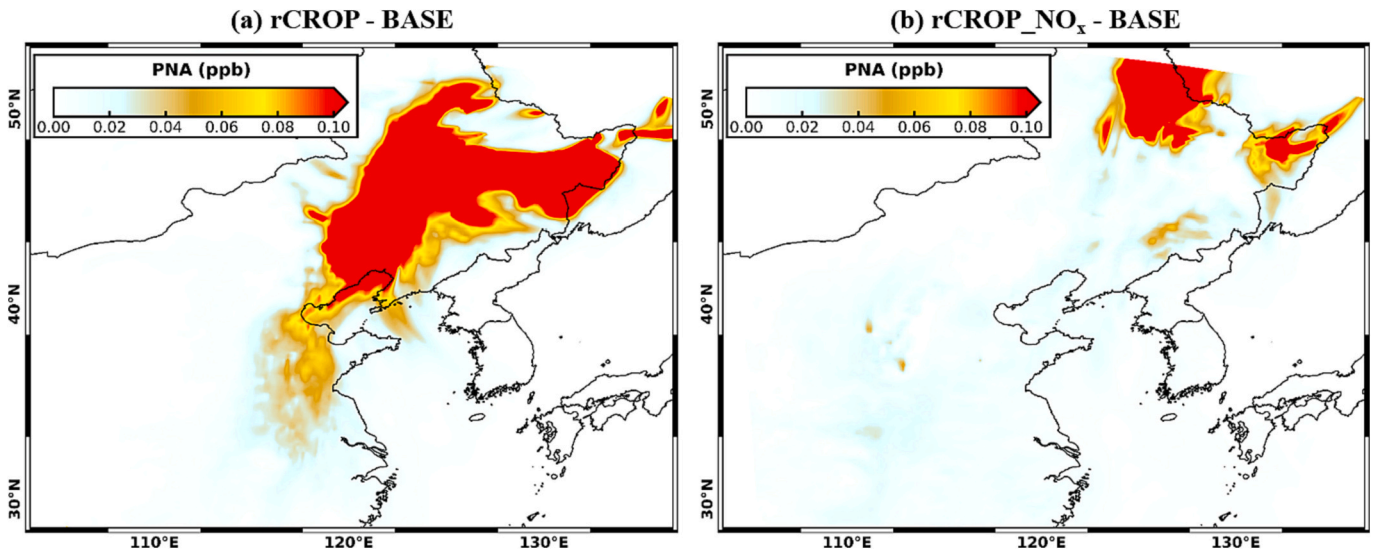

Fig. 7. Horizontal distribution of peroxynitric acid (PNA) concentration difference between each experiment (rCROP and rCROP_NO_x) and the BASE experiment. The values were averaged from the surface to the top of the plume during the analysis period.

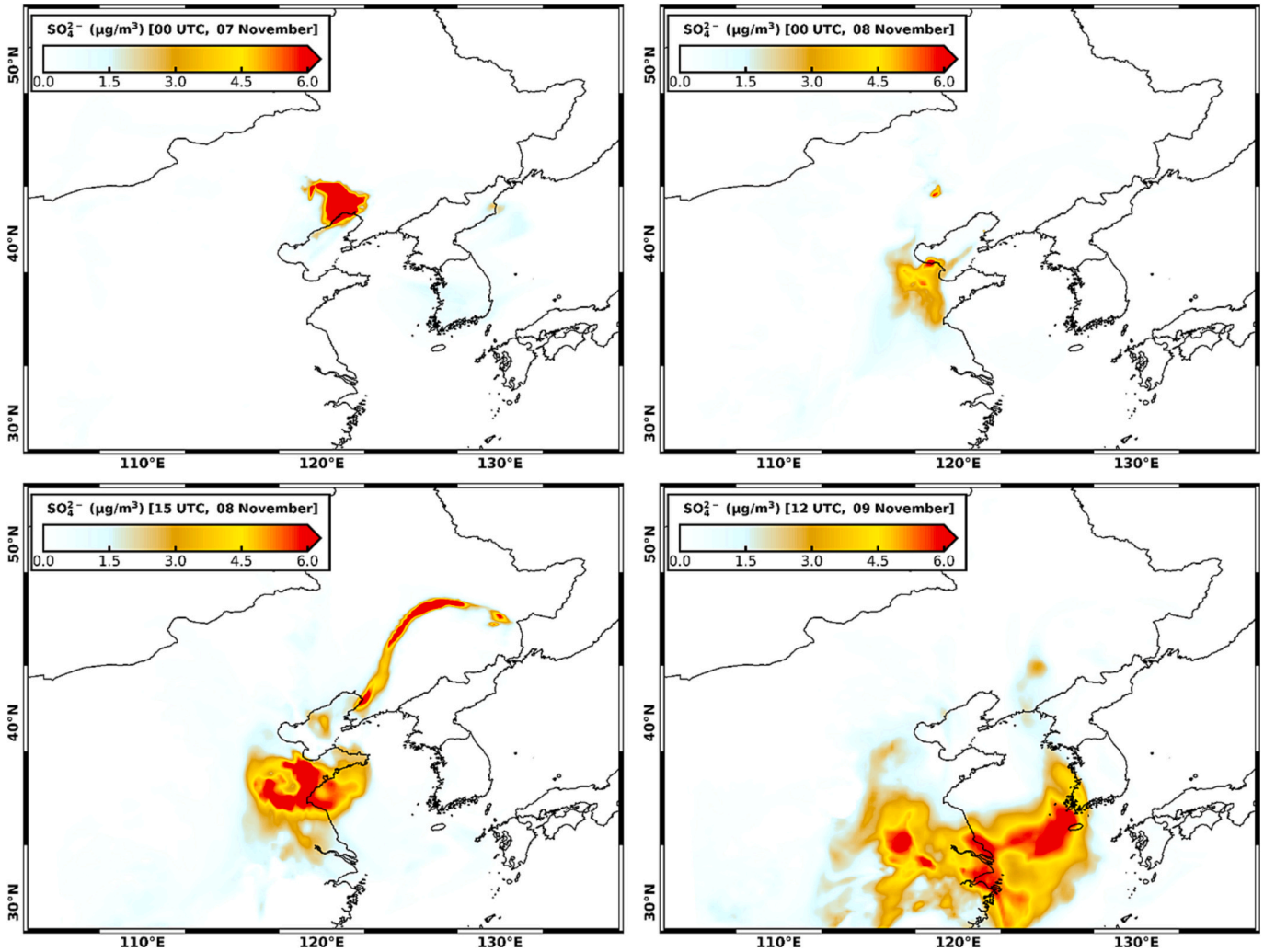

Fig. 8. Spatial transporting feature of the SO_4^{2-} concentration induced by crop burning. The values were averaged during the analysis period (unit: μg/m^3).

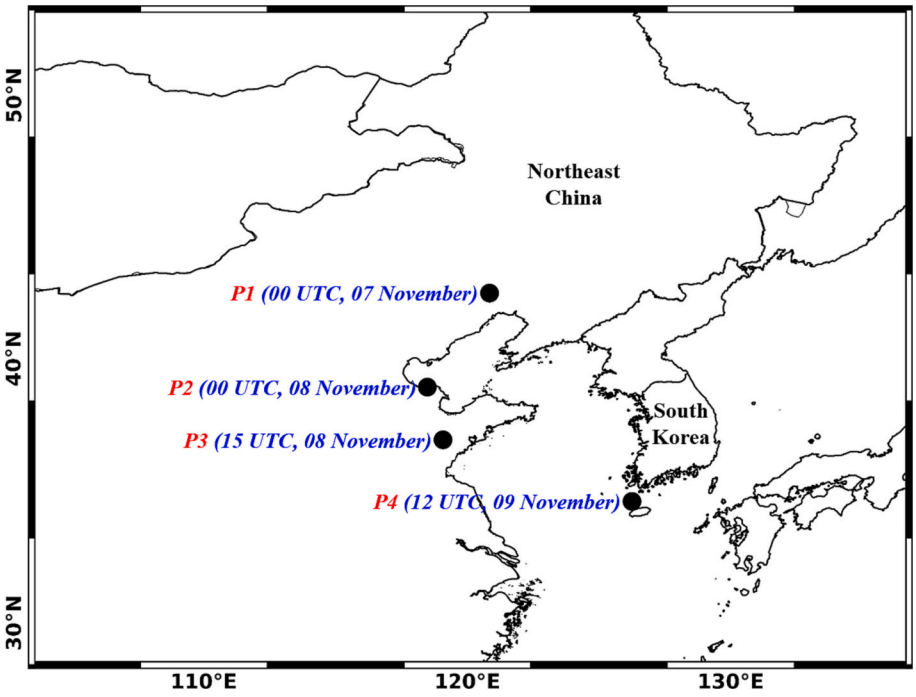

Fig. 9. Center locations of the SO_4^{2-} plume induced by crop burning at each hour.

Table 3
Concentration changes (μg/m^3) of each $PM_{2.5}$ component at the center locations shown in Fig. 9, and the proportion (%) of each component in the $PM_{2.5}$ concentrations.

	NO_3^-	SO_4^{2-}	NH_4^+	OC	EC	Others
P1	83.25 (26.22)	18.70 (5.89)	31.19 (9.82)	83.24 (26.22)	12.17 (3.83)	88.95 (28.02)
P2	58.85 (27.17)	6.38 (2.94)	19.37 (8.93)	58.14 (26.79)	8.89 (4.10)	65.40 (30.13)
P3	57.04 (31.37)	9.21 (5.07)	16.73 (9.20)	56.94 (31.32)	7.76 (4.27)	34.14 (18.78)
P4	6.75 (11.38)	7.42 (12.51)	4.52 (7.62)	18.76 (31.64)	2.19 (3.69)	19.66 (33.15)

Therefore, we conducted an additional IRR analysis of the HO_2. The HO_2 was mainly produced through the decomposition reaction of peroxynitric acid (PNA) (PNA = $HO_2 + NO_2$) (52.63%) (Gierczak et al., 2005; Bacak et al., 2011). Additionally, it was produced by a reaction involving VOCs and CO emitted from crop burning (30.04% and 7.84%, respectively).

In the chemical mechanism (CB6r3-AERO7) used in this study, PNA formation is determined by the reaction between HO_2 radicals and NO_2 ($HO_2 + NO_2 = PNA$) (Niki et al., 1977; Slusher et al., 2001; Cao et al., 2021). In this reaction, the NO_2 concentration, which is involved in PNA production, is influenced by NO_x emissions from crop burning. To explain the changes in PNA concentration caused by NO_x emissions, we conducted an additional sensitivity simulation that reduced the NO_x emissions by 50% (rCROP_NO_x) from the crop burning emissions used in the rCROP experiment. The PNA concentrations derived by calculating the difference between each experiment (rCROP, rCROP_NO_x) and the BASE experiment are shown in Fig. 7. The PNA concentration in Fig. 7(a) was high in Northeast China, where substantial crop burning occurred, as well as in East China. However, in Fig. 7(b), where NO_x emissions were reduced, the PNA concentration decreased overall. The decrease in NO_2 concentration, caused by the reduction in NO_x emissions in the rCROP_NO_x experiment, directly influenced the PNA production reaction, resulting in decreased PNA concentration. These results indicate that NO_x emissions from crop burning could impact the concentrations of H_2O_2, HO_2, and PNA, which are involved in SO_4^{2-} production. To summarize, NO_x emissions from crop burning contributed to the increased PNA concentration, and HO_2 generated through the PNA decomposition reaction led to the production of H_2O_2 during the transport of plumes. This transported H_2O_2 subsequently underwent a chemical reaction with abundant SO_2 in the vicinity of the Shandong Peninsula (Liu et al., 2018; Zhou et al., 2021), resulting in the formation of SO_4^{2-}. This SO_4^{2-} was then transported across the Yellow Sea, ultimately leading to elevated concentrations on Jeju Island. This suggests that NO_x emissions contribute substantially to the change in SO_4^{2-} concentration. Therefore, a comprehensive understanding of these reactions is essential to accurately analyze the mechanisms of SO_4^{2-} production.

3.5. Concentration proportion changes of $PM_{2.5}$ components during transport

We analyzed the concentration changes of $PM_{2.5}$ components resulting from crop burning emissions during their transport to Jeju Island in South Korea. The spatiotemporal behavior of SO_4^{2-} from Northeast China to Jeju Island is presented in Fig. 8, and Fig. 9 shows the locations where the highest concentrations of SO_4^{2-} were estimated at each time. Table 3 shows the concentration changes for $PM_{2.5}$ components at each location. The maximum concentration of SO_4^{2-} appeared in the northwestern region of the Korean Peninsula at 00 UTC on November 7 (P1). Subsequently, it was transported to the Shandong Peninsula in China (P2 and P3) and reached Jeju Island in South Korea at 09 UTC on November 9 (P4). At P1, all components of $PM_{2.5}$ exhibited their highest concentrations due to significant crop burning emissions. As the plume was transported to P4, the concentrations of NO_3^-, NH_4^+, OC, and EC rapidly decreased. In contrast, the SO_4^{2-} concentration increased at P3 (9.21 $\mu g/m^3$) compared to P2 (6.38 μg/m^3) due to the production reaction. The increased SO_4^{2-} concentration was sustained until P4 (7.42 μg/m^3) and affected the concentration proportions among $PM_{2.5}$ components. The proportion of SO_4^{2-} in the $PM_{2.5}$ concentrations at P1 was 5.89%, lower than NO_3^- (26.22%), NH_4^+ (9.82%), and OC (26.22%). However, owing to the transport of SO_4^{2-} produced in the Shandong Peninsula and the Yellow Sea, the SO_4^{2-} at P4 accounted for 12.51% of the $PM_{2.5}$ concentrations, higher than the proportions of NO_3^-

(11.38%) and NH_4^+ (7.62%). This was the second-highest among the $PM_{2.5}$ component concentrations at P4, following OC (31.64%). These findings suggest that the SO_4^{2-} produced by crop burning could significantly influence the $PM_{2.5}$ concentrations in downwind regions.

4. Conclusions

In this study, we analyzed the production mechanisms for each $PM_{2.5}$ component during the transport of pollutants from numerous crop burnings in Northeast China to the Korean Peninsula using the three-dimensional photochemical transport model CMAQ and crop burning emissions from the FINN data. The concentrations of NO_3^-, NH_4^+, OC, and EC among the major components of $PM_{2.5}$ were highest in Northeast China. In contrast, the SO_4^{2-} concentration increased in the Shandong Peninsula and remained high in the Yellow Sea, including Jeju Island. These results indicate that the SO_4^{2-} production process occurred during pollutant transport. The predominant mechanism for SO_4^{2-} production induced by crop burning emissions was the reaction $H_2O_2 + S(IV) = S(VI) + H_2O$ (1.44 μg/m^3, 80.49%). The H_2O_2, acting as a precursor to SO_4^{2-}, was primarily produced through the self-reaction of HO_2 radicals ($HO_2 + HO_2 = H_2O_2$, 54.32%, and $HO_2 + HO_2 + H_2O = H_2O_2$, 42.07%). Finally, HO_2 was mainly produced through the decomposition of PNA ($PNA = HO_2 + NO_2$, 52.63%), and the PNA concentration was found to be determined by the NO_x emissions from crop burning. The transported SO_4^{2-} reaching Jeju Island in South Korea changed the composition of $PM_{2.5}$. Although the proportion of SO_4^{2-} accounted for only 5.89% of $PM_{2.5}$ in Northeast China, it increased to 12.51% on Jeju Island. This demonstrates that the SO_4^{2-} produced by crop burning emissions could contribute to the proportion of SO_4^{2-} in observed $PM_{2.5}$ on Jeju Island.

Previous studies mainly attributed the production of SO_4^{2-} in the Yellow Sea to the oxidation of SO_2 by OH ($OH + SO_2 = SULF + HO_2$) (Jeon et al., 2018a, 2021). However, it is noteworthy that in this study, the production of SO_4^{2-} was found to be more prominently driven by the oxidation reaction involving H_2O_2 ($H_2O_2 + S(IV) = S(VI) + H_2O$) rather than that involving OH. Pollutants emitted from crop burning contributed to the production of PNA and HO_2, which subsequently formed H_2O_2, the precursors of SO_4^{2-}. This cascade of reactions suggests the necessity for a comprehensive understanding of the mechanisms of PNA and HO_2 production, alongside H_2O_2, to accurately predict the production reactions of SO_4^{2-} resulting from crop burning emissions.

CRediT authorship contribution statement

Dongjin Kim: Conceptualization, Formal analysis, Methodology, Writing – original draft. **Yunsoo Choi:** Supervision, Writing – review & editing. **Wonbae Jeon:** Conceptualization, Formal analysis, Supervision, Writing – review & editing. **Jeonghyeok Mun:** Investigation, Software, Validation. **Jaehyeong Park:** Investigation, Visualization, Writing – review & editing. **Cheol-Hee Kim:** Funding acquisition, Project administration. **Jung-Woo Yoo:** Writing – review & editing.

Declaration of competing interest

The authors declare that they have no known competing financial interests or personal relationships that could have appeared to influence the work reported in this paper.

Data availability

Data will be made available on request.

Acknowledgments

This research was partially supported by the Basic Science Research Program through the National Research Foundation of Korea (NRF) funded by the Ministry of Education (NRF-2020R1A6A1A03044834) and the National Research Foundation of Korea (NRF) grant funded by the Korea Government (MSIT) (No. 2023R1A2C1002608).

Appendix A. Supplementary data

Supplementary data to this article can be found online at https://doi.org/10.1016/j.atmosres.2024.107303.

References

Akagi, S.K., Yokelson, R.J., Wiedinmyer, C., Alvarado, M.J., Reid, J.S., Karl, T., Crounse, J.D., Wennberg, P.O., 2011. Emission factors for open and domestic biomass burning for use in atmospheric models. Atmos. Chem. Phys. 11, 4039–4072. https://doi.org/10.5194/acp-11-4039-2011.

Akagi, S.K., Craven, J.S., Taylor, J.W., McMeeking, G.R., Yokelson, R.J., Burling, I.R., Urbanski, S.P., Wold, C.E., Seinfeld, J.H., Coe, H., Alvarado, M.J., Weise, D.R., 2012. Evolution of trace gases and particles emitted by a chaparral fire in California. Atmos. Chem. Phys. 12, 1397–1421. https://doi.org/10.5194/acp-12-1397-2012.

Appel, K.W., Bash, J.O., Fahey, K.M., Foley, K.M., Gilliam, R.C., Hogrefe, C., Hutzell, W. T., Kang, D., Mathur, R., Murphy, B.N., Napelenok, S.L., Nolte, C.G., Pleim, J.E., Pouliot, G.A., Pye, H.O.T., Ran, L., Roselle, S.J., Sarwar, G., Schwede, D.B., Sidi, F.I., Spero, T.L., Wong, D.C., 2021. The Community Multiscale Air Quality (CMAQ) model versions 5.3 and 5.3.1: system updates and evaluation. Geosci. Model Dev. 14, 2867–2897. https://doi.org/10.5194/gmd-14-2867-2021.

Bacak, A., Cooke, M.C., Bardwell, M.W., McGillen, M.R., Archibald, A.T., Huey, L.G., Tanner, D., Utembe, S.R., Jenkin, M.E., Derwent, R.G., Shallcross, D.E., Percival, C. J., 2011. Kinetics of the $HO_2 + NO_2$ Reaction: On the impact of new gas-phase kinetic data for the formation of HO_2NO_2 on HO_x, NO_x and HO_2NO_2 levels in the troposphere. Atmos. Environ. 45 (35), 6414–6422. https://doi.org/10.1016/j.atmosenv.2011.08.008.

Bae, C., Kim, B.-U., Kim, H.C., Yoo, C., Kim, S., 2020. Long-range transport influence on key chemical components of $PM_{2.5}$ in the Seoul metropolitan area, South Korea, during the years 2012–2016. Atmosphere 11, 48. https://doi.org/10.3390/atmos11010048.

Byun, D., Schere, K.L., 2006. Review of the governing equations, computational algorithms, and other components of the Models-3 Community Multiscale Air Quality (CMAQ) modeling system. Appl. Mech. Rev. 59 (2), 51–77. https://doi.org/10.1115/1.2128636.

Cao, Z., Zhou, X., Ma, Y., Wang, L., Wu, R., Chen, B., Wang, W., 2017. The concentrations, formations, relationships and modeling of sulfate, nitrate and ammonium (SNA) aerosols over China. Aerosol Air Qual. Res. 17, 84–97. https://doi.org/10.4209/aaqr.2016.01.0020.

Cao, L., Li, S., Sun, L., 2021. Study of different Carbon Bond 6 (CB6) mechanisms by using a concentration sensitivity analysis. Atmos. Chem. Phys. 21, 12687–12714. https://doi.org/10.5194/acp-21-12687-2021.

Chen, Y., Li, D., Karimian, H., Wang, S., Fang, S., 2022. The relationship between air quality and MODIS aerosol optical depth in major cities of the Yangtze River Delta. Chemosphere 308, 136301. https://doi.org/10.1016/j.chemosphere.2022.136301.

Cheng, Y., Yu, Q.Q., Liu, J.M., Zhu, S.Q., Zhang, M.Y., Zhang, H.L., Zheng, B., He, K.B., 2021. Model vs. observation discrepancy in aerosol characteristics during a half-year long campaign in Northeast China: the role of biomass burning. Environ. Pollut. 269, 116167 https://doi.org/10.1016/j.envpol.2020.116167.

Chu, D.A., Kaufman, Y.J., Zibordi, G., Chern, J.D., Mao, J., Li, C., Holben, B.N., 2003. Global monitoring of air pollution over land from the Earth observing system-terra moderate resolution imaging spectroradiometer (MODIS). J. Geophys. Res. 108, 4661. https://doi.org/10.1029/2002JD003179.

Crippa, M., Guizzardi, D., Muntean, M., Schaaf, E., Monforti-Ferrario, F., Banja, M., Pagani, F., Solazzo, E., 2022. EDGAR v6.1 global air pollutant emissions. In: European Commission. JRC129555. http://data.jrc.ec.europa.eu/collection/edgar.

Draxler, R.R., 1999. HYSPLIT4 user's guide. In: NOAA Tech. Memo, ERL ARL-230. NOAA Air Resources Laboratory, Silver Spring, MD. https://www.arl.noaa.gov/wp_arl/wp-content/uploads/documents/reports/arl-230.pdf.

Feng, Z., Wang, X., Yuan, J., Zhang, Y., Yu, M., 2023. Changes in air pollution, land surface temperature, and urban heat islands during the COVID-19 lockdown in three Chinese urban agglomerations. Sci. Total Environ. 892, 164496 https://doi.org/10.1016/j.scitotenv.2023.164496.

Friedl, M.A., Sulla-Menashe, D., Tan, B., Schneider, A., Ramankutty, N., Sibley, A., Huang, X., 2010. MODIS collection 5 global land cover: algorithm refinements and characterization of new datasets. Remote Sens. Environ. 114, 168–182. https://doi.org/10.1016/j.rse.2009.08.016.

Friedman, B., Brophy, P., Brune, W.H., Farmer, D.K., 2016. Anthropogenic sulfur perturbations on biogenic oxidation: SO_2 additions impact gas-phase OH oxidation products of α-and β-pinene. Environ. Sci. Technol. 50, 1269–1279. https://doi.org/10.1021/acs.est.5b05010.

Gierczak, T., Jimenez, E., Riffault, V., Burkholder, J.B., Ravishankara, A.R., 2005. Thermal decomposition of HO_2NO_2 (peroxynitric acid, PNA): rate coefficient and determination of the enthalpy of formation. J. Phys. Chem. A 109, 586–596. https://doi.org/10.1021/jp046632f.

Gipson, G.L., 1999. Process analysis. In: Byun, D.W., Ching, J.K.S. (Eds.), Science Algorithms of the EPA Models-3 Community Multiscale Air Quality (CMAQ) Modeling System. U.S. Environmental Protection Agency, Washington, D.C.. EPA/600/R-99/030 (NTISPB2000-100561).

Guenther, A., Jiang, X., Heald, C.L., Sakulyanontvittaya, T., Duhl, T., Emmons, L., Wang, X., 2012. The Model of Emissions of Gases and Aerosols from Nature version 2.1 (MEGAN2. 1): an extended and updated framework for modeling biogenic emissions. Geosci. Model Dev. 5, 1471–1492. https://doi.org/10.5194/gmd-5-1471-2012.

Hong, X., Zhang, C., Tian, Y., Wu, H., Zhu, Y., Liu, C., 2023. Quantification and evaluation of atmospheric emissions from crop residue burning constrained by satellite observations in China during 2016–2020. Sci. Total Environ. 865, 161237 https://doi.org/10.1016/j.scitotenv.2022.161237.

Itahashi, S., Yamaji, K., Chatani, S., Hayami, H., 2018. Refinement of modeled aqueous-phase sulfate production via the Fe-and Mn-catalyzed oxidation pathway. Atmosphere 9, 132. https://doi.org/10.3390/atmos9040132.

Jeon, W., Choi, Y., Lee, H.W., Lee, S.H., Yoo, J.W., Park, J., 2015. A quantitative analysis of grid nudging effect on each process of $PM_{2.5}$ production in the Korean Peninsula. Atmos. Environ. 122, 763–774. https://doi.org/10.1016/j.atmosenv.2015.10.050.

Jeon, W., Choi, Y., Mun, J., Lee, S.H., Choi, H.J., Yoo, J.W., Lee, H.J., Lee, H.W., 2018a. Behavior of sulfate on the sea surface during its transport from Eastern China to South Korea. Atmos. Environ. 186, 102–112. https://doi.org/10.1016/j.atmosenv.2018.05.017.

Jeon, W., Choi, Y., Souri, A.H., Roy, A., Diao, L., Pan, S., Lee, H.W., Lee, S.-H., 2018b. Identification of chemical fingerprints in long-range transport of burning induced upper tropospheric ozone from Colorado to the North Atlantic Ocean. Sci. Total Environ. 613, 820–828. https://doi.org/10.1016/j.scitotenv.2017.09.177.

Jeon, W., Park, J., Choi, Y., Mun, J., Kim, D., Kim, C.-H., Lee, H.-J., Bak, J., Jo, H.-Y., 2021. The mechanism of the formation of high sulfate concentrations over the Yellow Sea during the KORUS-AQ period: The effect of transport/atmospheric chemistry and ocean emissions. Atmos. Res. 261, 105756 https://doi.org/10.1016/j.atmosres.2021.105756.

Johnson, M.S., Strawbridge, K., Knowland, K.E., Keller, C., Travis, M., 2021. Long-range transport of Siberian biomass burning emissions to North America during FIREX-AQ. Atmos. Environ. 252 https://doi.org/10.1016/j.atmosenv.2021.118241.

Kai, Z., Yuesi, W., Tianxue, W., Yousef, M., Frank, M., 2007. Properties of nitrate, sulfate and ammonium in typical polluted atmospheric aerosols (PM_{10}) in Beijing. Atmos. Res. 84, 67–77. https://doi.org/10.1016/j.atmosres.2006.05.004.

Kim, J.Y., Lee, J.Y., Choi, S.-D., Kim, Y.P., Ghim, Y.S., 2012. Gaseous and particulate polycyclic aromatic hydrocarbons at the Gosan background site in East Asia. Atmos. Environ. 49, 311–319. https://doi.org/10.1016/j.atmosenv.2011.11.029.

Kim, H.C., Kim, E., Bae, C., Cho, J.H., Kim, B.-U., Kim, S., 2017. Regional contributions to particulate matter concentration in the Seoul metropolitan area, South Korea: seasonal variation and sensitivity to meteorology and emissions inventory. Atmos. Chem. Phys. 17, 10315–10332. https://doi.org/10.5194/acp-17-10315-2017.

Kim, D., Jeon, W., Park, J., Mun, J., Choi, H., Kim, C.-H., Lee, H.-J., Jo, H.-Y., 2022. A numerical analysis of the changes in O_3 concentration in a wildfire plume. Remote Sens. 14, 4549. https://doi.org/10.3390/rs14184549.

Kyung, S.Y., Jeong, S.H., 2020. Particulate-matter related respiratory diseases. Tuberc. Respir. Dis. 83 (2), 116–121. https://doi.org/10.4046/trd.2019.0025.

Lee, T., Choi, J., Lee, G., Ahn, J., Park, J.S., Atwood, S.A., Schurman, M., Choi, Y., Chung, Y., Collett, J.L., 2015a. Characterization of aerosol composition, concentrations, and sources at Baengnyeong Island, Korea using an aerosol mass spectrometer. Atmos. Environ. 120, 297–306. https://doi.org/10.1016/j.atmosenv.2015.08.038.

Lee, K., Kim, Y.J., Kang, C.H., Kim, J.S., Chang, L.S., Park, K., 2015b. Chemical characteristics of long-range-transported fine particulate matter at Gosan, Jeju island, in the spring and fall of 2008, 2009, 2011, and 2012. J. Air Waste Manage. Assoc. 65 (4), 445–454. https://doi.org/10.1080/10962247.2014.1001883.

Lee, J.-J., Lee, J.-B., Kim, O., Heo, G., Lee, H., Lee, D., Kim, D.-G., Lee, S.-D., 2021. Crop residue burning in Northeast China and its impact on $PM_{2.5}$ concentrations in South Korea. Atmosphere 12, 1212. https://doi.org/10.3390/atmos12091212.

Lee, H.-J., Jo, Y.-J., Kim, S., Kim, D., Kim, J.-M., Choi, D., Jo, H.-Y., Bak, J., Park, S.-Y., Jeon, W., Kim, C.-H., 2022. Transboundary aerosol transport process and its impact on aerosol-radiation-cloud feedbacks in springtime over Northeast Asia. Sci. Rep. 12, 4870. https://doi.org/10.1038/s41598-022-08854-1.

Levy, R., Hsu, C., Sayer, A., Mattoo, S., Lee, J., 2017. MODIS Atmosphere L2 Aerosol Product. NASA MODIS Adaptive Processing System, Goddard Space Flight Center. https://doi.org/10.5067/MODIS/MYD04_L2.061.

Li, L., Yan, D., Xu, S., Huang, M., Wang, X., Xie, S., 2017. Characteristics and source distribution of air pollution in winter in Qingdao, Eastern China. Environ. Pollut. 224, 44–53. https://doi.org/10.1016/j.envpol.2016.12.037.

Lin, C.-Y., Zhao, C., Liu, X., Lin, N.-H., Chen, W.-N., 2014. Modelling of long-range transport of Southeast Asia biomass-burning aerosols to Taiwan and their radiative forcings over East Asia. Tellus B 66, 23733. https://doi.org/10.3402/tellusb.v66.23733.

Liu, Y., Warner, T.T., Bowers, J.F., Carson, L.P., Chen, F., Clough, C.A., Davis, C.A., Egeland, C.H., Halvorson, S., Huck Jr., T.W., Lachapelle, L., Malone, R.E., Rife, D.L., Sheu, R.-S., Swerdlin, S.P., Weingarten, D.S., 2008. The operational mesogamma-scale analysis and forecast system of the US Army Test and Evaluation Command. Part 1: Overview of the modeling system, the forecast products. J. Appl. Meteorol. Climatol. 47, 1077–1092. https://doi.org/10.1175/2007JAMC1653.1.

Liu, X.H., Zhang, Y., Xing, J., Zhang, Q., Wang, K., Streets, D.G., Jang, C.J., Wang, W.X., Hao, J.M., 2010. Understanding of regional air pollution over China using CMAQ, Part II. Process analysis and sensitivity of ozone and particulate matter to precursor emissions. Atmos. Environ. 44, 3719–3727. https://doi.org/10.1016/j.atmosenv.2010.03.036.

Liu, H., Wu, B., Liu, S., Shao, P., Liu, X., Zhu, C., Yong, W., Wu, Y., Xue, Y., Gao, J., Hao, Y., Tian, H., 2018. A regional high-resolution emission inventory of primary air pollutants in 2012 for Beijing and the surrounding five provinces of North China. Atmos. Environ. 181, 20–33. https://doi.org/10.1016/j.atmosenv.2018.03.013.

Moon, K.J., Han, J.S., Ghim, Y.S., Kim, Y.J., 2008. Source apportionment of fine carbonaceous particles by positive matrix factorization at Gosan background site in East Asia. Environ. Int. 34 (5), 654–664. https://doi.org/10.1016/j.envint.2007.12.021.

Niki, H., Maker, P.D., Savage, C.M., Breitenbach, L.P., 1977. Fourier transform IR spectroscopic observation of pernitric acid formed via $HOO + NO_2 \rightarrow HOONO_2$. Chem. Phys. Lett. 45, 564–566. https://doi.org/10.1016/0009-2614(77)80090-0.

Otte, T.L., Pleim, J.E., 2010. The Meteorology-Chemistry Interface Processor (MCIP) for the CMAQ modeling system: updates through MCIPv3.4.1. Geosci. Model Dev. 3, 243–256. https://doi.org/10.5194/gmd-3-243-2010.

Sarwar, G., Godowitch, J., Henderson, B.H., Fahey, K., Pouliot, G., Hutzell, W.T., Mathur, R., Kang, D., Goliff, W.S., Stockwell, W.R., 2013. A comparison of atmospheric composition using the Carbon Bond and Regional Atmospheric Chemistry Mechanisms. Atmos. Chem. Phys. 13, 9695–9712. https://doi.org/10.5194/acp-13-9695-2013.

Si, Y., Wang, H., Cai, K., Chen, L., Zhou, Z., Li, S., 2019. Long-term (2006–2015) variations and relations of multiple atmospheric pollutants based on multi-remote sensing data over the North China Plain. Environ. Pollut. 255, 113323 https://doi.org/10.1016/j.envpol.2019.113323.

Skamarock, W.C., Klemp, J.B., Dudhia, J., Gill, D.O., Liu, Z., Berner, J., Wang, W., Powers, J.G., Duda, M.G., Barker, D., Huang, X.-Y., 2019. A Description of the Advanced Research WRF Version 4. National Center for Atmospheric Research, Boulder, CO, USA, p. 145.

Slusher, D.L., Pitteri, S.J., Haman, B.J., Tanner, D.J., Huey, L.G., 2001. A chemical ionization technique for measurement of pernitric acid in the upper troposphere and the polar boundary layer. Geophys. Res. Lett. 28, 3875–3878. https://doi.org/10.1029/2001GL013443.

Stauffer, D.R., Seaman, N.L., 1990. Use of four-dimensional data assimilation in a limited area mesoscale model. Part I: Experiments with synoptic-scale data. Mon. Weather Rev. 118, 1250–1277. https://doi.org/10.1175/1520-0493(1990)118<1250:UOFDDA>2.0.CO;2.

Stein, A.F., Draxler, R.R., Rolph, G.D., Stunder, B.J.B., Cohen, M.D., Ngan, F., 2015. NOAA's HYSPLIT atmospheric transport and dispersion modeling system. Bull. Amer. Meteor. Soc. 96, 2059–2077. https://doi.org/10.1175/BAMS-D-14-00110.1.

Stockwell, W.R., 1995. On the $HO_2 + HO_2$ reaction: Its misapplication in atmospheric chemistry models. J. Geophys. Res. 100 (D6), 11695–11698. https://doi.org/10.1029/94JD03107.

Uranishi, K., Ikemori, F., Shimadera, H., Kondo, A., Sugata, S., 2019. Impact of field biomass burning on local pollution and long-range transport of $PM_{2.5}$ in Northeast Asia. Environ. Pollut. 244, 414–422. https://doi.org/10.1016/j.envpol.2018.09.061.

Val Martin, M., Honrath, R.E., Owen, R.C., Pfister, G., Fialho, P., Barata, F., 2006. Significant enhancements of nitrogen oxides, black carbon, and ozone in the North Atlantic lower free troposphere resulting from North American boreal wildfires. J. Geophys. Res. 111, D23S60. https://doi.org/10.1029/2006JD007530.

Wiedinmyer, C., Akagi, S.K., Yokelson, R.J., Emmons, L.K., Al-Saadi, J.A., Orlando, J.J., Soja, A.J., 2011. The Fire INventory from NCAR (FINN): a high resolution global model to estimate the emissions from open burning. Geosci. Model Dev. 4, 625–641. https://doi.org/10.5194/gmd-4-625-2011.

Xie, Q., Sun, Q., 2021. Monitoring the spatial variation of aerosol optical depth and its correlation with land use/land cover in Wuhan, China: a perspective of urban planning. Int. J. Environ. Res. Public Health 18 (3), 1132. https://doi.org/10.3390/ijerph18031132.

Xu, Q., Li, X., Wang, S., Wang, C., Huang, F., Gao, Q., Wu, L., Tao, L., Guo, J., Wang, W., 2016. Fine particulate air pollution and hospital emergency room visits for respiratory disease in urban areas in Beijing, China, in 2013. PLoS One 11 (4), e0153099. https://doi.org/10.1371/journal.pone.0153099.

Xu, R., Tie, X., Li, G., Zhao, S., Cao, J., Feng, T., Long, X., 2018. Effect of biomass burning on black carbon (BC) in South Asia and Tibetan Plateau: the analysis of WRF-Chem modeling. Sci. Total Environ. 645, 901–912. https://doi.org/10.1016/j.scitotenv.2018.07.165.

Yadav, I.C., Devi, N.L., 2019. Biomass burning, regional air quality, and climate change. Enc. Env. Hlth. 386–391. https://doi.org/10.1016/B978-0-12-409548-9.11022-X.

Yamaji, K., Li, J., Uno, I., Kanaya, Y., Irie, H., Takigawa, M., Komazaki, Y., Pochanart, P., Liu, Y., Tanimoto, H., Ohara, T., Yan, X., Wang, Z., Akimoto, H., 2010. Impact of open crop residual burning on air quality over Central Eastern China during the Mount Tai Experiment 2006 (MTX2006). Atmos. Chem. Phys. 10, 7353–7368. https://doi.org/10.5194/acp-10-7353-2010.

Yeo, M.J., Kim, Y.P., 2019. Trends of the PM_{10} concentrations and high PM_{10} concentration cases in Korea. J. Korean Soc. Atmos. Environ. 35 (2), 249–264. https://doi.org/10.5572/KOSAE.2019.35.2.249.

Yin, S., Wang, X., Zhang, X., Guo, M., Miura, M., Xiao, Y., 2019a. Influence of biomass burning on local air pollution in mainland Southeast Asia from 2001 to 2016. Environ. Pollut. 254, 112949 https://doi.org/10.1016/j.envpol.2019.07.117.

Yin, S., Wang, X., Zhang, X., Zhang, Z., Xiao, Y., Tani, H., Sun, Z., 2019b. Exploring the effects of crop residue burning on local haze pollution in Northeast China using ground and satellite data. Atmos. Environ. 199, 189–201. https://doi.org/10.1016/j.atmosenv.2018.11.033.

Zhang, J., Liu, L., Wang, Y.Y., Ren, Y., Wang, X., Shi, Z.B., Zhang, D.Z., Che, H.Z., Zhao, H.J., Liu, Y.F., Niu, H.Y., Chen, J.M., Zhang, X.Y., Lingaswamy, A.P., Wang, Z. F., Li, W.J., 2017. Chemical composition, source, and process of urban aerosols during winter haze formation in Northeast China. Environ. Pollut. 231, 357–366. https://doi.org/10.1016/j.envpol.2017.07.102.

Zhou, Y., Xing, X., Lang, J., Chen, D., Cheng, S., Wei, L., Wei, X., Liu, C., 2017. A comprehensive biomass burning emission inventory with high spatial and

temporal resolution in China. Atmos. Chem. Phys. 17, 2839–2864. https://doi.org/10.5194/acp-17-2839-2017.

Zhou, L.X., Baker, K.R., Napelenok, S.L., Pouliot, G., Elleman, R., O'Neill, S.M., Urbanski, S.P., Wong, D.C., 2018a. Modeling crop residue burning experiments to evaluate smoke emissions and plume transport. Sci. Total Environ. 627, 523–533. https://doi.org/10.1016/j.scitotenv.2018.01.237.

Zhou, Y., Han, Z., Liu, R., Zhu, B., Li, J., Zhang, R., 2018b. A modeling study of the impact of crop residue burning on $PM_{2.5}$ concentration in Beijing and Tianjin during a severe autumn haze event. Aerosol Air Qual. Res. 18, 1558–1572. https://doi.org/10.4209/aaqr.2017.09.0334.

Zhou, M., Jiang, W., Gao, W., Gao, X., Ma, M., Ma, X., 2021. Anthropogenic emission inventory of multiple air pollutants and their spatiotemporal variations in 2017 for the Shandong province, China. Environ. Pollut. 288, 117666 https://doi.org/10.1016/j.envpol.2021.117666.